Energy level alignment of a hole-transport organic layer and ITO: Towards applications for organic electronic devices

Quentin Arnoux, Anthony Boucly, Vincent Barth, Rabah Benbalagh, Albano Cossaro, Luca Floreano, Mathieu G Silly, Fausto Sirotti, Etienne Derat, Stephane Carniato, et al.

Energy level alignment of a hole-transport organic layer and ITO: Towards applications for organic electronic devices

Quentin ARNOUX,[1,2,3,] Anthony BOUCLY,[1] Vincent BARTH,[2,3,4] Rabah BENBALAGH,[1] Albano COSSARO,[5] Luca FLOREANO,[5] Mathieu SILLY,[6] Fausto SIROTTI,[6] Etienne DERAT,[2] Stéphane CARNIATO,[1] Fabrice BOURNEL,[1,6] Jean-Jacques GALLET,[1,6] Denis FICHOU,[2,4,7] Ludovic TORTECH,[2,3,*] François ROCHET.[1,6,*]*

[1] Sorbonne Universités, UPMC Univ Paris 06, UMR 7614, Laboratoire de Chimie Physique Matière et Rayonnement (LCPMR), F-75005 Paris, France.

[2] Sorbonne Universités, UPMC Univ Paris 06, UMR 8232, Institut Parisien de Chimie Moléculaire (IPCM), F-75005, Paris, France.

[3] CEA Saclay, IRAMIS, NIMBE (UMR 3685), Laboratoire d'Innovation en Chimie des Surfaces et Nanosciences (LICSEN), F-91191 Gif-sur-Yvette, France.

[4] CNRS, UMR 8232, Institut Parisien de Chimie Moléculaire (IPCM), F-75005, Paris, France.

[5] CNR-IOM, Istituto Officina dei Materiali, TASC Laboratory, S.S. 14, km 163.5, 34149, Basovizza, Italy

[6] Synchrotron SOLEIL, L'Orme des Merisiers, Saint-Aubin, BP 48, F-91192 Gif-sur-Yvette, France.

[7] School of Physical and Mathematical Sciences (SPMS), Nanyang Technological University, Singapore 637371, Singapore.

* Corresponding authors: quentin.arnoux@upmc.fr, ludovic.tortech@upmc.fr, francois.rochet@upmc.fr

Abstract

2,2',6,6'-tetraphenyl-4,4'-dipyranylidene (DIPO-Ph_4) was grown by vacuum-deposition on an indium tin oxide (ITO) substrate. The films were characterized by atomic force microscopy and synchrotron radiation UV and X-ray photoelectron spectroscopy to gain an insight into the material growth and to better understand the electronic properties of the ITO/DIPO-Ph_4 interface. To interpret our spectroscopic data, we consider the formation of cationic DIPO-Ph_4 at ITO interface owing to a charge transfer from the organic layer to the substrate. Ionization energy DFT calculations of the neutral and cationic species substantiate this hypothesis. Finally, we present the energetic diagram of the ITO/DIPO-Ph_4 system, and discuss the application of this interface in various technologically relevant systems, as a hole-injector in OLEDs or as a hole-collector interfacial layer adjacent to the prototypical OPV layer P3HT:PCBM.

Keywords

Organic solar cells, Interfacial layer, Hole-transport layer, Metal/Organic interface, Photoemission spectroscopy, Charge transfer

Introduction

The materials of the transparent electrodes (anodes) of the organic photovoltaic (OPV) devices are mainly oxides,[1–3] although a replacement with alternative materials, for instance polymers[4] and graphene,[5–7] starts to be explored. Among the oxides, Sn-doped In_2O_3 (indium tin oxide, ITO) still remains the dominant material despite its high cost in front of alternative oxides like aluminum-doped zinc oxides,

mainly because of a better resistance to degradation in outdoor environments.[8] In fact, those types of oxides present detrimental effect on the power conversion efficiency of organic solar cells because of their sensitivity to acidic condition, or because they may induce the degradation of the active layer.

To improve the durability and the efficiency of the OPV, interfacial layers (IFLs) are used to bridge morphologically and electronically the electrode and the active layer. The IFL is made of organic materials (polymers, small molecules), of graphene oxide[9] or even of inorganic material like NiO.[10] It is systematically deposited between the ITO electrode and the standard photovoltaic active layers (often a P3HT:PCBM blend).[11] The most widely used IFL is the PEDOT:PSS polymer because of its high conductivity and easy processability, but its high acidity can lead to ITO deterioration.[11] To circumvent this difficulty some of the present authors have explored the benefit of depositing a hole-transport molecular solid of the dipyranylidene (DIP) family (2,2',6,6'-tetraphenyl-4,4'-dithiapyranylidene, DIPS-Ph_4) on ITO to finally form an ITO/DIPS-Ph_4/P3HT:PCBM/LiF/Al cell in which the short-circuit density (J_{SC})[12] is efficiently increased. Current sensing contact mode atomic force microscopy (CS-AFM) shows that there is a considerable increase in the total number of hole-carrying pathways with respect to a PEDOT:PSS IFL.[12]

The reason of the hole-collection efficiency lies, besides interface morphological aspects, in the favorable alignment of the energy levels of the molecular solid with the ITO band structure. However, it is worth noticing that the formation of the interface between ITO and a molecular film is often oversimplified in the literature on OPV and this because of two reasons.

First, the electronic levels of the conductive oxide and of the molecular materials are most often placed against each other by aligning the vacuum levels (the so-called Schottky-Mott limit). A vast literature on metal/organic or on inorganic semiconductor/organic interfaces shows that it is far to be always the case.[13–19] Various models were proposed. In the integer charge transfer model, according to the respective energies of the metal work function and of donor/acceptor polaronic levels related to, but not confounded with, the highest occupied molecular orbital (HOMO)/lowest unoccupied molecular orbital (LUMO) level, charge can be transferred across the interface or not. When charge transfer occurs, the energy levels

are pinned by the acceptor/donor polaronic levels. A change in the work function is seen and the Schottky-Mott alignment is not observed.[16] The concept of the polaronic level, on which the integer charge transfer model was based, was recently challenged by the electrostatic model of Oehzelt and coworkers[19] who considered the polaronic energy as almost negligible. Relying heavily on the density of state (DOS) of the organic film, the spatial profile of the electrostatic potential in the organic layer was calculated via the Poisson equation. Briefly, when charge transfer occurs the HOMO (donor case) (or LUMO, for the acceptor case) aligns with the Fermi level of the metal very close to the surface, and further apart an extended "band-bending" region appears, according to the DOS. The electrostatic model of Ref. 19 reproduces the experimental behavior of the hole- and electron-injection barriers versus the substrate work function, distinguishing cases obeying the Schottky-Mott limit from those where the HOMO or LUMO of the molecular solid pin the work function.

Second, ITO is also often depicted as an "ordinary" metal. In fact, it is an n-type degenerate wide gap semiconductor. The value of the direct gap E_G of In_2O_3 has evolved with time, from $\sim$ 3.6 eV in the earlier publications (based on optical spectra, see Ref. 20) to a much smaller value of $\sim$ 2.8 – 2.9 eV (X-ray photoelectron spectroscopy (XPS), ab-initio band structure calculations[21] and scanning tunneling spectroscopy[22]). The filling of the conduction band, according to the Burstein-Moss model[23,24] is realized via the presence of Sn donors substituting In atoms (up to $\sim$ 0.3 eV from its bottom[25]). ITO being a semiconductor the question has raised as of whether a depletion layer, chemical (due to an oxygen gradient influencing the doping) or physical (due to the accumulation of negative charge at the surface), occurs in the layers close to the surface.[20] Indeed an upward band bending at the surface can be detrimental for the collection of holes (the injection of electrons) at the interface with the IFL. The value of E_G greatly determined the existence of a depletion layer. In contrast to the conclusions of the UV photoelectron spectroscopy (UPS) work of Gassenbauer *et al.* (Ref. 20) where an E_G of $\sim$ 3.6 eV was considered, the most recent high energy XPS study of the valence-band, at 3.6 keV photon energy,[21] points to a flat band situation extending deeply in the bulk (the electron escape depth is $\sim$ 6 nm) together

with a low E_G value of ~ 2.8 eV. A subsequent high energy XPS analysis at 6 keV of the In 3d core levels is indicative of a slight carrier depletion in the layers closer to the surface.[26]

The present study examines the growth of a molecular solid 2,2',6,6'-tetraphenyl-4,4'-dipyranylidene (DIPO-Ph_4, Figure 1) on ITO substrates. Indeed DIPO-Ph_4 is a promising molecule to create an effective hole-conducting IFL at the transparent anode in OPV.[27] It forms a high-conductivity donor-acceptor complex with tetracyanoquinodimethane (TCNQ).[28] Its oxidation potential of 0.24 V (relative to ferrocene) makes it a better electron donor than tetrathiafulvalene (TTF). Its ionization energy is ~ 4.6 eV, according to Forrest's relationship.[29] In the solid state, the optical gap is ~ 2 eV (see Figure S1 in SI Section S1). The geometry of the free molecule is depicted in Figure 1: the four phenyls are almost parallel to the dipyranylidene core, the dihedral angle being ~ 18°.[30] In the solid state, molecules pack plane-to-plane in columns and the dihedral angle of the phenyl groups reduces to 7.6 – 10.2°.[31]

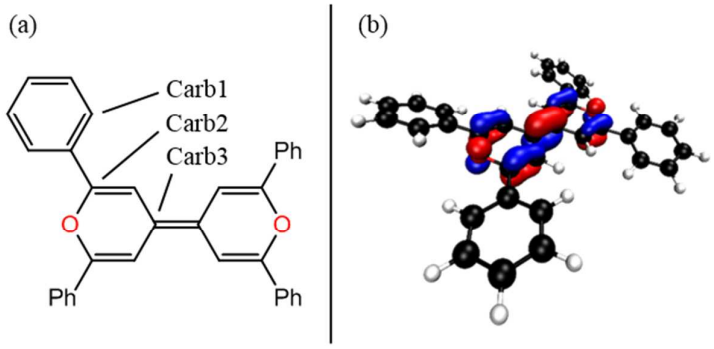

Figure 1. (a) DIPO-Ph_4 structure and carbons place used for DFT calculation; (b) DFT geometric optimization of the free DIPO-Ph_4 molecule (dark, white, and red spheres correspond to C, H, and O atoms respectively) and HOMO representation.

Prior to molecular deposition, the ITO surface is submitted to a chemically cleaning procedure, that leaves a weak carbon contamination and give a relatively low work function[32] (4 eV). This surface treatment was preferred to the standard UV ozone cleaning, that is responsible for the degradation of molecular layers due to the formation of active oxygen.[33] Then DIPO-Ph_4 is deposited on chemically cleaned commercial ITO substrates in ultra-high vacuum (UHV) conditions by thermal evaporation. Synchrotron radiation core-level photoelectron spectroscopy (XPS) and valence-band spectroscopy (UPS) are carried out, immediately after the deposition to give clues on the chemical bond, charge state and on

the alignment of the energy levels at the interface.[17,34] As DIPO-Ph_4 is an excellent donor,[28] complementary density functional theory (DFT) calculations of core ionization energies of the molecule in the neutral and cationic states are performed to estimate the XPS binding energy shift. Changes in the morphology of the deposits with increasing average thicknesses are monitored (*ex situ*) by atomic force microscopy (AFM). Due to the non-continuous film formation, the latter analysis helps understanding the evolution of the photoemission spectra. Finally, the performance of the DIPO-Ph_4 film as a hole collector layer is discussed against the backdrop of new information on the electronic structure and growth morphology provided by the present study.

1 Experimental

1.1 DIPO-Ph_4 synthesis and chemical characterization

DIPO-Ph_4 has been prepared following a synthesis the CEA team developed.[35] The final compound was characterized via Nuclear Magnetic Resonance (NMR) and via elementary analysis (see Table S1 in SI Section S2). There is no contamination detected.

1.2 Sample preparation at TEMPO beamline

All DIPO-Ph_4 deposits are prepared on commercial ITO substrate (SOLEMS) having a sheet resistance of 25 $\Omega \cdot sq^{-1}$. After DECON 90 treatment, the ITO substrates were cleaned ultrasonically in bathes of dichloromethane and propan-2-ol (10 min each) without any further treatment before DIPO-Ph_4 deposition. After its introduction into the ultra-high vacuum ($\sim 10^{-10}$ mbar) preparation chamber, the ITO substrate was exposed to a molecular beam of DIPO-Ph_4 using a Knudsen cell positioned at 4 cm from it. The molecular beam was slightly tilted A quartz balance (QB) monitor allows us to follow the deposition rate. The substrate is kept at room temperature. Several deposits are made, characterized by the average number of molecules per cm^2: 1×10^{15}, 2×10^{15}, 3×10^{15} and 8×10^{15} molecule$\cdot cm^{-2}$. The DIPO-Ph_4 covered

substrates are then introduced in the XPS analysis chamber of TEMPO beamline in a pressure better than $\sim 10^{-10}$ mbar.

1.3 Photoemission spectroscopies

Most of the photoemission data were collected at TEMPO beamline, SOLEIL synchrotron, France. The synchrotron light spot of the TEMPO beamline is defocused to 1 mm × 2 mm purposely to decrease the photon flux, and to avoid beam damage, without losing photoelectron count rate. The electron analyzer is a modified SCIENTA200 machine fitted with a delay line detector. All photoemission spectra are taken with a take-off angle of 0° with respect to the surface normal. Valence band spectra and shallow core-levels (Sn 4d, In 4d) are recorded at $h\nu$ = 60 eV in surface sensitive conditions. The In 4d and Sn 4d spectra are also recorded in more bulk sensitive conditions at 825 eV to profile out the Sn distribution in the material. In 3d core-levels were measured at 600 eV. C 1s, O 1s core-level XPS spectra were respectively recorded at $h\nu$ = 340 eV and $h\nu$ = 600 eV with an overall experimental resolution better than 100 meV. After subtraction of a Shirley background, the spectra are reconstructed with sums of Voigt functions, with respectively a 340, 380, 80, 150, 199 and 210 meV Lorentzian full widths at half maximum (FWHM, corresponding to the core-hole lifetime) for Sn 3d, In 3d, C 1s, O 1s, In 4d and Sn 4d, respectively, according to the literature.[36] The Gaussian contribution, that may change according to the chemical environment, is indicated in the text. It is worth to notice that the value of core/valence level width σ_{i} can be determined according to Hwang *et al.* work:[37]

$$\sigma_{\mathrm{i}} = \sqrt{{\sigma_{\mathrm{XPS/UPS}}}^2 - {\sigma_{\mathrm{inst}}}^2 - {\sigma_{\mathrm{surf}}}^2 - {\sigma_{\mathrm{vib}}}^2} \qquad \textbf{(1)}$$

Surface relaxation processes (σ_{surf}) and vibrational coupling (σ_{vib}) are estimated to be both in the range of 0.05 – 0.2 eV.[37] The instrumental resolution (σ_{inst}) is measured at the Fermi edge of a clean metal sample (σ_{inst}(Au) = 0.08 eV). σ_{i} can be then used as a key value for the determination of the effective injection barrier.[38]

The variation curve of the inelastic mean free path versus the kinetic energy of the photoelectron was calculated for ITO using TPP-2M method.[39,40] It is given as Figure S2 in the supporting information. Binding energies (BE) are referenced with respect to the Fermi level (E_F) determined from a scrapped area of the copper sample holder in electrical contact with the ITO substrate. The work function was determined by measuring the kinetic energy (KE) of the secondary electron cutoff (KE_{CO}). To avoid truncating the spectrum by the analyzer work-function, the sample was negatively biased (to -20 V) with respect to the analyzer. The knowledge of KE_{CO}, that of the kinetic energy of the Fermi level (KE_{FL}) measured on the metallic contact, and the precise determination of the photon energy $h\nu$ (using 1st and 2nd order core level peaks), enables the determination of the work function Φ of the sample as $\Phi = h\nu - (KE_{FL} - KE_{CO})$.

Complementary XPS characterization of the bare ITO surface were also carried at ALOISA beamline out using synchrotron light (ELETTRA synchrotron Facility, Trieste, Italy) and at Laboratoire de Chimie Physique Matière et Rayonnement (LCPMR, Paris), where a standard laboratory setup was used (a PHOIBOS 150 analyzer from SPECS and a non-monochromatized Al K_α source).

1.4 Atomic force microscopy (AFM)

The surface morphology of the DIPO-Ph_4 films deposited in the TEMPO beamline preparation chamber is investigated *ex situ* via Atomic Force Microscopy (AFM) at CEA (IRAMIS group). The AFM used is a Molecular Imaging from Agilent, PicoLE, used in contact mode using a conductive Pt/Ir tip of radius 20 nm. The spring constant of the cantilever is 0.2 $N{\cdot}m^{-1}$. The vertical resolution in contact mode is 0.5 nm. The sample roughness is determined thanks to root mean square method (RMS).

2 Results and discussion

2.1 DIPO-Ph_4 layer morphology studied via AFM

Atomic force microscopy (AFM) is used to examine those samples that were previously examined by photoelectron spectroscopies. As the knowledge of the morphology of the deposited layer is instrumental to interpret correctly our XPS/UPS data, the AFM images (shown in Figure 2) are discussed first.

The chemical cleaning is efficient as the bare ITO surface appears without particle contamination. Yet, after the chemical cleaning process, ring-shaped structures remain on ITO surface. They are characterized by an average height of 2 nm and an average diameter of 100 nm (Figure 2(a)). They cover 20% of the surface. Away from these "craters", the roughness remains low ($\pm$ 0.65 nm).

The DIPO-Ph_4 coverage is monitored during the evaporation in the preparation chamber of TEMPO beamline via a quartz balance (QB-coverage). The weight increase per surface unit is converted into a molecular surface density using the density given by Chasseau *et al.*.[31] After the deposition of 10^{15} molecule·cm^{-2} , the AFM image (Figure 2(b_1)) shows that 3D clusters ("mounds") cover 25% of ITO surface. The average height of the cluster is 30 nm with an average diameter of 150 nm. Given the cluster density, an average volume of DIPO-Ph_4 per surface unit is obtained, leading to a molecular surface density of 0.94×10^{15} molecule·cm^{-2} (using the density of Ref. 31) in excellent agreement with the QB-coverage. These clusters grow from nucleation points situated at the side of the ring-shaped features. For the 3×10^{15} molecule·cm^{-2} deposit (QB-coverage), the DIPO-Ph_4 layer covers now 60% of the ITO surface. The 3D growth of circular mounds switches to that of recumbent, elongated (needle-like) mounds. Their average height remains ~ 30 nm, as for the 10^{15} molecule·cm^{-2} deposit, with typical lateral and longitudinal dimensions of ~ 150 and ~ 400 nm. The molecular coverage deduced from the AFM image is $2.80\cdot10^{15}$ molecule·cm^{-2}, also in accord with the QB measurement. Finally, we show the AFM image (Figure 2(d_1)) and profile (Figure 2(d_2)) of the "thick" layer, corresponding to a deposit of 8×10^{15} molecule·cm^{-2}. The film covers now more than 95% of the ITO surface, and its average thickness is ~ 43 nm.

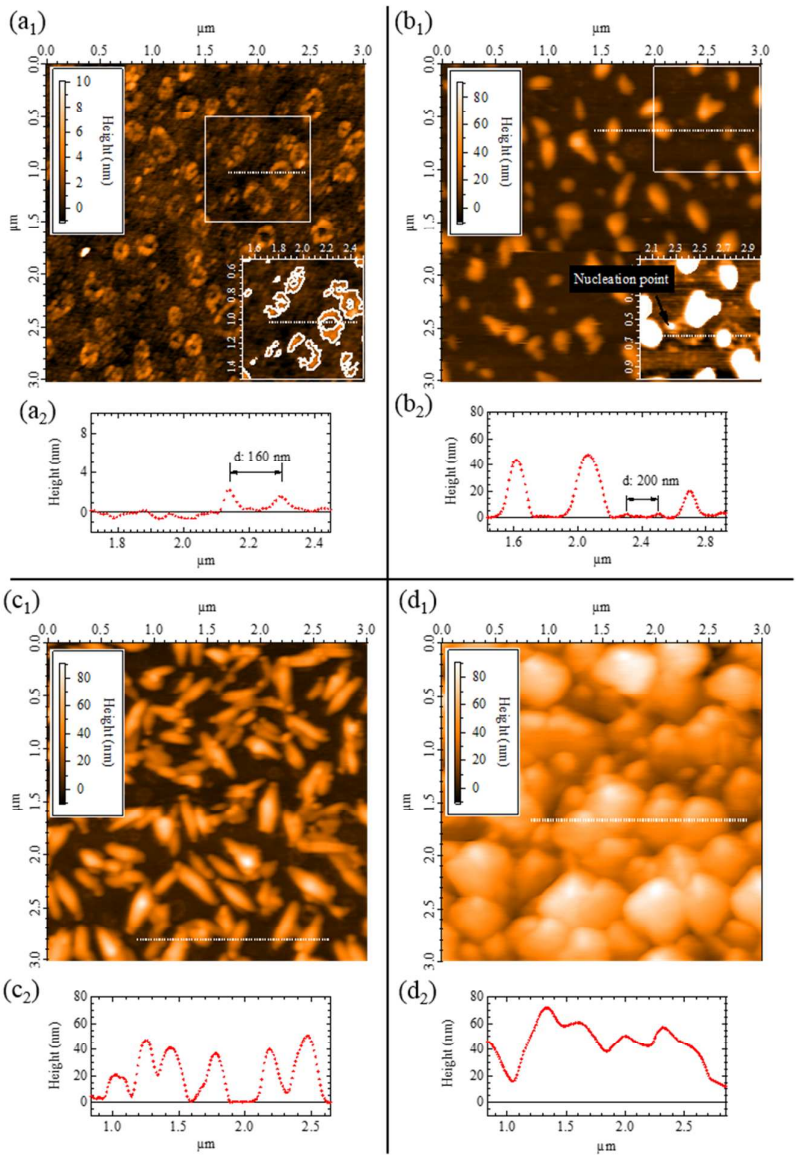

Figure 2. AFM images: (a_1) Chemically cleaned ITO presenting ring-shaped features; (b_1) QB-coverage of 1×10^{15} molecule.cm^{-2}; (c_1) QB-coverage 3×10^{15} molecule·cm^{-2}; (d_1) QB coverage 8×10^{15} molecule·cm^{-2}; (a_2), (b_2), (c_2) and (d_2) are the profiles indicated by the dotted straight lines in (a_1), (b_1), (c_1), and (d_1) respectively. The molecular coverage, expressed in molecule·cm^{-2} (QB-coverage), is obtained from a quartz balance measurement.

When layers are deposited over homogeneous substrates, like single crystals, two types of growth are classically considered. In a Volmer-Weber[41] growth, the organic molecules cluster in islands, leaving bare substrate areas. This arises from the fact that the interaction between molecules (π-stacking) is much stronger than the interaction between the DIPO-Ph$_4$ molecule and the ITO substrate. Alternately, in a Stranski-Krastanov growth,[41] the molecule-molecule interaction competes with molecule-substrate

interactions. A thin wetting layer covers all the substrate, on top of which the 3D island growth mode takes place. If a Stranski-Krastanov mode stands, then given that the crater-like defects of the ITO substrate remain visible (Figure 2(b_2)), the wetting layer, if present, should not exceed ~ 2 nm.

In the present case, the growth mode may be more complicated as numerous, 10 to 100 nm size defects (the calderas) are found on the surface, that serve as starting point for the mound growth. The flanks of the mounds themselves cannot be abrupt, and a significant "aureole" may surround the mounds, with a thickness comparable to the XPS probing depths (≤ 1 nm).

2.2 Core-level XPS spectroscopy

The In $3d_{5/2}$ spectra of the bare, chemically cleaned surface are given in Figure S3 and Table S2. The value of the first plasmon component energy ($\hbar\omega_p$ ~ 0.75 eV) measured in surface sensitive conditions ($h\nu$ = 600 eV, kinetic energy of 155 eV, λ_{ITO} ~ 0.56 nm) enables an estimate of the carrier density, about 4×10^{20} cm^{-3}.[42] Both the changes in $\hbar\omega_p$ and the Sn/In atomic ratio deduced from the In 4d and Sn 4d peaks as a function of the probing depth (using various excitation energies, see Figure S4 and Table S3, SI Section S5) suggest an accumulation of Sn dopants in the near surface region (Sn/In equal to 0.13 at the surface, and 0.10 more in the bulk), in agreement with previous observations.[20]

The deposition of the DIPO-Ph_4 molecule affects the In $3d_{5/2}$ BE. After the first deposit (10^{15} molecule·cm^{-2}, see Figure S3), the In $3d_{5/2}$ peak ($h\nu$ = 600 eV) moves to higher binding energy by 100 meV. This indicates that the energy difference between the Fermi level and the conduction band minimum increases. According to the AFM images, DIPO-Ph_4 is in the form of mounds, of thickness ~ 30 nm, separated by inter-mound areas. Thus, given the IMFP (~ 0.56 nm), most of the In 3d signal comes from the inter-mound areas (75% of the surface) and from thin aureoles around the mounds. The observed BE shift means that molecules interacting with ITO surface change slightly the surface charge density:[43] an electronic transfer from the molecule to the substrate could explain the motion of the Fermi

with respect to conduction band minimum. For subsequent depositions (for which the inter-mound area recedes down to 40%), the position of the In $3d_{5/2}$ peak does not change any more, showing that the Fermi level remains anchored at the position reached after the first deposit.

The C1s XPS spectra of the ITO surface, bare and covered by the molecule are shown in Figure 3 and Table 1. The C 1s of the bare sample is due to contamination. It presents the characteristic peak of an aliphatic carbon at ~ 284.9 eV.[44] The C 1s/In $3d_{5/2}$ intensity ratio, measured at $h\nu$ = 600 eV (KE C 1s ~ 315 eV, $\lambda_{\mathrm{DIPO\text{-}Ph_4}}$ ~ 1.19 nm) is 16% for the chemical cleaned ITO. Then it rises to 65, 79, 139 and 2364% for the QB coverages of 1×10^{15}, 2×10^{15}, 3×10^{15} and 8×10^{15} molecule·cm^{-2}, respectively. These ratio values indicate that the C 1s spectra are characteristic of the deposited film.

The C 1s spectra does not exhibit any BE shift, from 1×10^{15} to 3×10^{15} molecule·cm^{-2}, indicating that the position of the Fermi level remains constant in the organic material while the mounds are laterally growing. The C 1s spectra are fitted with three Voigt components: one main component labelled C1 at ~ 285 eV, with a FWHM of ~ 1.2 eV and two weaker peaks, one labelled C2 at ~ 286 eV and one labelled C3 at 287.5 eV. Peak C1 has the typical BE expected for aryl carbons. A more thorough examination of the BEs will be made after the discussion of the O 1s spectra, here below. C2 peak is attributed to C bonded to oxygen atoms and C3 one at ~ 1.5 eV higher BE that is likely a shakeup. The spectral weight of the C–O component is 0.15, 0.13, 0.09 and 0.11 for the 1×10^{15}, 2×10^{15}, 3×10^{15} and 8×10^{15} molecule·cm^{-2} respectively. Note that the aryl carbons and core carbons not bonded to O atoms represent 70.5% and 17.6% of the carbon atoms (88% in all), while the carbons in ether bonds amount to 12%.

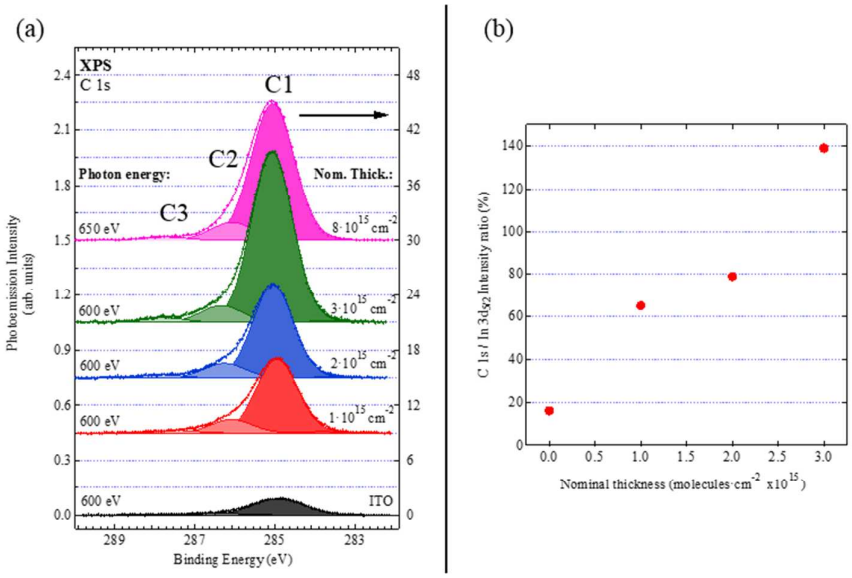

Figure 3. (a) C 1s spectra of the chemically cleaned ITO substrate, bare and covered with increasing QB-coverages of DIPO-Ph_4 (1×10^{15}, 2×10^{15}, 3×10^{15} and 8×10^{15} molecule·cm^{-2}); (b) C 1s / In $3d_{5/2}$ intensity evolution with the increase of QB-coverage. The C 1s intensity is normalized according to In $3d_{5/2}$ intensity.

Table 1. C 1s main component BE and Gaussian FWHM (G-FWHM) obtained from fits of the spectra given in Figure 3.The core-hole lifetime Lorentzian FWHM (L-FWHM) is 80 meV for C 1 s. DIPO-Ph_4 coverages (in molecule·cm^{-2}) are deduced from QB measurements. The C 1s to In $3d_{5/2}$ intensity ratio is also given.

Samples		Phot. Energy	G-FWHM	Peak C1 (eV)	Peak C2 (eV)	$r_{C2/(C1+C2)}$	C 1s / In $3d_{5/2}$ ratio
Chemically cleaned ITO		825 eV	1.657 eV	284.91	_	_	8 %
		600 eV	1.488 eV	284.92	_	_	16 %
	1×10^{15} molecule·cm^{-2}	600 eV	1.168 eV	284.96	286.09	0.15	65 %
	2×10^{15} molecule·cm^{-2}	600 eV	1.156 eV	284.96	286.26	0.13	79 %
	3×10^{15} molecule·cm^{-2}	600 eV	1.180 eV	285.08	286.34	0.09	139 %
	8×10^{15} molecule·cm^{-2}	650 eV	1.222 eV	285.06	286.00	0.11	2364 %

The O 1s core-level spectra of the chemically cleaned bare ITO surface (Figure 4 and Table 2) are measured at $h\nu$ = 825 eV (KE O 1s ~ 295 eV, λ_{ITO} ~ 0.79 nm) and at $h\nu$ = 600 eV (KE O 1s ~ 70 eV, λ_{ITO} ~ 0.47 nm). In both cases, the spectra are fitted with four components of equal widths. In more bulk sensitive conditions ($h\nu$ = 825 eV) the BE of peak I (42% of the spectra weight), II (31%), III (22%) and IV (6%) are 530.17, 530.81, 531.78 and 532.89 eV, respectively. Peak II (0.6 eV from peak I) can be

attributed to a plasmon loss, as also observed in the In $3d_{5/2}$ spectra (Figure S3). Peak III (1.6 eV from peak I) could correspond to the second plasmon or to organic contamination.[45] Finally peak IV may be attributable to surface hydroxyls, that are expected in the range 532.5 – 532.9 eV.[45,46] In more surface sensitive conditions ($h\nu$ = 600 eV), peaks I (51%), II (31%), III (15%) and IV (3%) are found at 530.30, 531.38, 532.37, 533.48, respectively. The second observation is the increased BE shift (1.07 eV instead of 0.75 eV) between peak I and peak II. This is reminiscent of what is observed for the plasmon loss energy in the In $3d_{5/2}$ spectra that is greater at the surface than in the bulk. However, 1.07 eV is a too large value for the plasmon energy. It is likely that peak II encompasses both the plasmon peak and a component due to defects (*e.g.* suboxides[45]), the latter being more abundant at the surface. Surface contamination by oxygenated species can be estimated from the atomic ratio $r_{\mathrm{O/In}}$ ($\lambda_{\mathrm{ITO}} \sim 0.47 - 0.56$ nm) The latter is calculated from O 1s intensity and In 3d at $h\nu$ = 600 eV, corrected from cross-section variations. $r_{\mathrm{O/In}}$ is $\sim$ 1.8, very close to 1.7, the value expected for the In_2O_3 stoichiometry. This indicates that the contribution of the oxygen contamination is small.

We consider now the changes induced on the O1s spectrum by the deposition of DIPO-Ph_4. The O 1s spectrum measured at $h\nu$ = 600 eV in "surface sensitive conditions" (KE O 1s $\sim$ 70 eV, $\lambda_{\mathrm{ITO}} \sim 0.47$ nm and $\lambda_{\mathrm{DIPO\text{-}Ph_4}} \sim 0.55$ nm) are given in Figure 4(a). As the substrate contains oxygen, the spectra of the DIPO-Ph_4 covered ITO surface are fitted by a sum of Voigt components that reproduces the bare ITO spectral shape, to which two new components, due to the DIPO-Ph_4 molecule are added. As shown in Figure 4, the O1 and O2 components appear at $\sim$ 532.2 eV and $\sim$ 533.6 eV, respectively. We have also verified that the appearance of O2 is not trivially due to beam damage (see Figure S5) during the XPS measurements.

The subtraction of the bare ITO contribution emphasizes the molecular solid contribution. In Figure 4(b) we give the difference spectra obtained in surface sensitive condition ($KE \sim 70$ eV, $\lambda_{\mathrm{DIPO\text{-}Ph_4}} \sim 0.55$ nm) and in bulk sensitive ones ($KE \sim 293$ eV, $\lambda_{\mathrm{DIPO\text{-}Ph_4}} \sim 1.14$ nm, the original spectra are given in Figure S6). In fact, in DIPO-Ph_4 the two oxygen atoms are chemically equivalent (see Figure 1), and thus one single O 1s contribution should be observed. Indeed peak O1 is found at the typical BE of the C–O–C

ether bond, in the range 531.5 – 532 eV, according to literature.[47] The O 1s spectrum ($h\nu$ = 650 eV, $\lambda_{\text{DIPO-Ph}_4}$ ~ 0.6 nm) of thick DIPO-Ph$_4$ deposit (8×10^{15} molecule·cm^{-2}) is the one for which the contribution of the substrate (the grey shaded component) is the least, see Figure 4(c). It exhibits the O1 and the O2 components at 534.27 eV (with $r_{\text{O2/(O1+O2)}}$ = 0.16, see Table 2).

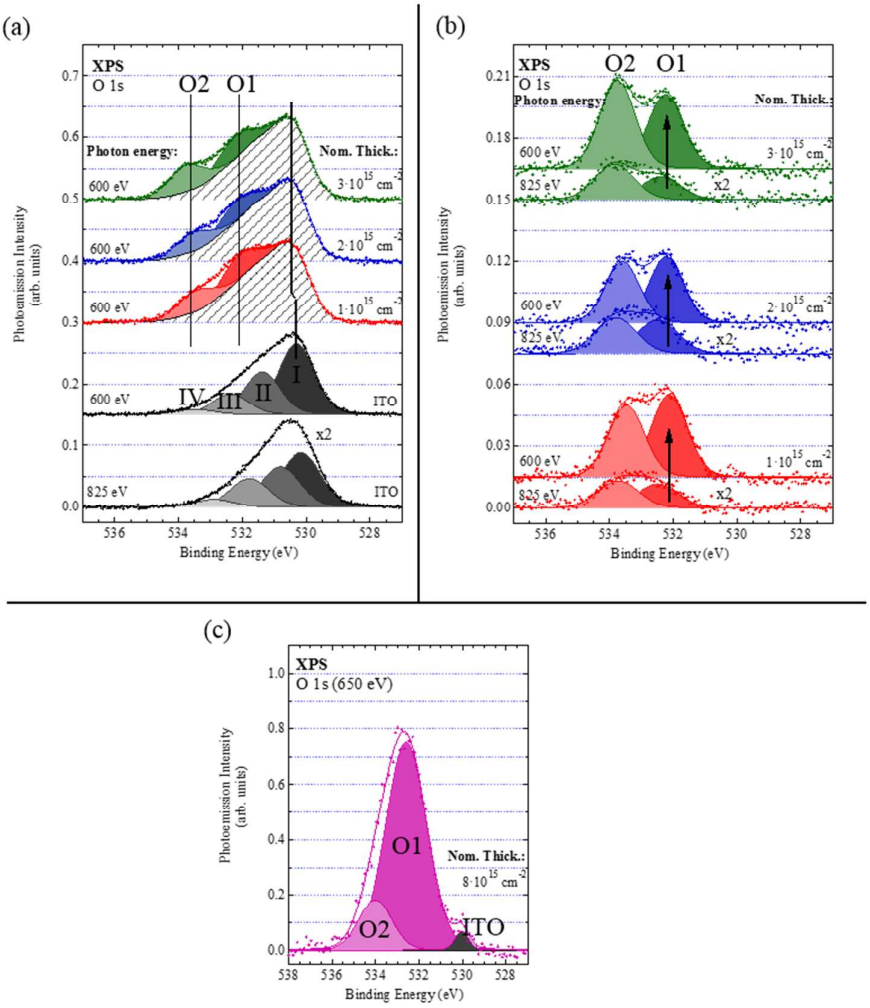

Figure 4. (a) O 1s spectra of the chemically cleaned ITO substrate, bare and covered with increasing QB-coverages of DIPO-Ph$_4$ (1×10^{15}, 2×10^{15} and 3×10^{15} molecule·cm^{-2}). The molecular solid contribution comprises two new components O1 and O2 added to the "synthetized" bare ITO spectrum. The spectra shown in (b) are obtained by subtraction of the ITO substrate contribution to the spectra shown in (a), emphasizing the contribution of DIPO-Ph$_4$. Coverages are obtained from QB measurements. (c) The O 1s spectrum of the thickest deposit measured at photon energy of 650 eV. The grey shaded component arises from the ITO substrate.

Table 2. O 1s *BE* and Gaussian FWHM (G-FWHM) of the main peaks obtained by fitting the spectra given in Figure 4. The Lorentzian width (L-FWHM) is 150 meV for the O 1s peaks. $r_{\text{O2/(O1+O2)}}$ measures

the O2 ($BE \sim 533.6 \pm 0.1$ eV) contribution weight in the molecule-related spectral intensity Coverages are obtained from QB measurements.

Samples		Phot. Energy	G-FWHM	Peak I (eV)	Peak O1 (eV)	Peak O2 (eV)	$r_{O2/(O1+O2)}$
Chemically cleaned ITO		825 eV	1.370 eV	530.17	_	_	_
		600 eV	1.239 eV	530.30	_	_	_
	1×10^{15} molecule·cm^{-2}	825 eV	1.436 eV	530.39	532.48	533.72	0.53
		600 eV	1.252 eV	530.46	532.13	533.47	0.46
	2×10^{15} molecule·cm^{-2}	825 eV	1.433 eV	530.43	532.40	533.70	0.52
		600 eV	1.196 eV	530.42	532.12	533.50	0.48
	3×10^{15} molecule·cm^{-2}	825 eV	1.378 eV	530.39	532.39	533.84	0.61
		600 eV	1.227 eV	530.48	532.24	533.75	0.54
	8×10^{15} molecule·cm^{-2}	650 eV	_	_	532.84	534.27	0.16

The observation of two oxygen components can find various explanations. Let us examine the more trivial explanations. First the used material introduced in the crucible may contain a high proportion of oxygen containing molecules co-evaporated with DIPO-Ph_4. This must be discarded as the purity of the material was checked by NMR and elementary analysis (see experimental details Table S1, Section S2). Second, the presence of background impurities co-adsorbed with DIPO-Ph_4, is not realistic as the evaporation was carried out in a UHV system. Therefore, we must consider that the molecule is present in two different forms, one corresponding to the unaltered molecule, with an ether O 1s component labelled O1, and one corresponding to an altered form, characterized by the O2 component. Any interpretation of the O2 component should be consistent with the fitting of the C 1s spectrum into two components (attributed to ester carbons and carbons not bonded to oxygen) that corresponds to the DIPO-Ph_4 stoichiometry.

The molecule can be altered by a chemical reaction with species released by the ITO substrate. Indeed, aggressive oxygenated species on the ITO substrate (*e.g.* generated by UV ozone treatments) can break the bonds of organic molecules and oxidize them.[48] The C–O bond of the ether moiety may break leading to the insertion of further oxygens. Indeed, BE of 532.2 and 533.7 eV are found for the carbonyl and ether type oxygens in ester groups of polymers, respectively.[47] Against this view, there is no indication for a carboxylic/carboxylate peak at ~ 289 eV in the C 1s spectrum as shown in Figure 3, and the $r_{O2/(O1+O2)}$

ratio is not fixed at 0.5. Other species could diffuse away from the substrate. For instance indium atoms are reported to penetrate deeply into molecular solids such as PTCDA when an indium metal layer is deposited upon it.[49] Tin atoms are less prone to diffuse into PTCDA.[50] The presence of indium in the molecular solid should be noticed by new components appearing in the In $3d_{5/2}$ spectrum when the DIPO-Ph_4 is added, which is not the case (In $3d_{5/2}$ spectrum of the 8×10^{15} molecule·cm^{-2} sample). The same observation can be made for the Sn 3d peak that is not affected by DIPO-Ph_4 deposition (see SI, Figure S7), apart from a $+100$ meV BE shift after deposition of the first layer (10^{15} molecule·cm^{-2}).

The hypothesis alternative to the chemical reaction is that of a charge transfer from the molecule (a good donor[28]) to the ITO substrate or to some acceptor species present in the deposited films. This leads to the formation of the radical cation $[\text{DIPO-Ph}_4]^{\bullet+}$.

This hypothesis is further explored by calculating the O 1s BE shift between the cationic and the neutral molecule in the gas phase (we consider a single molecule) using DFT (Table 3). Details on the method are given in the SI, Section S9 and in previous papers by our group.[51–53] Calculations of C, N and O 1s ionization potentials of a series of molecules were shown to be precise to better than 0.1 eV when compared to the experimental gas-phase values.[51,53–55] The calculated O 1s ionization energy (IE_{core}, *i.e.* the BE referenced to the vacuum level) of the neutral molecule ($IE_{\text{core}}^{\text{neutral,gas}}$) is 537.64 eV, while that of the molecular cation ($IE_{\text{core}}^{\text{cation,gas}}$) in the triplet state is 541.42 eV. Via a Hartree-Fock (HF) calculation, we have checked that the singlet state $IE_{\text{core}}^{\text{cation,gas}}$ that contributes to 1/3 of the spectra weight is very close in energy to the triplet state, *i.e.* only 0.08 eV higher in energy, see Table S4, SI Section S9. Therefore, the triplet and singlet states should be merged into one in the experimental spectra, given the resolution.

The difference of $\sim$ 3.8 eV between the cationic (triplet) and neutral state DFT ionization energies is much larger than the O2−O1 BE difference of 1.5 eV we measure for the molecular solid. In fact, as shown in the SI, Section S10, a simple dielectric response model describes the relaxation energy effects via the polarization energy P of a unit charge. Then the cationic-neutral BE shift is reduced in the solid

state with respect to the gas phase due to core-hole screening by the dielectric medium in the final state. It comes that:

$$BE_{\text{core}}^{\text{cation,solid}} - BE_{\text{core}}^{\text{neutral,solid}} = (IE_{\text{core}}^{\text{cation,gas}} - IE_{\text{core}}^{\text{neutral,gas}}) - 2P \quad \textbf{(2)}$$

where $IE_{\text{core}}^{\text{cation,solid}}$ and $IE_{\text{core}}^{\text{neutral,solid}}$ are the ionization energies (measured from the vacuum level) in the solid of the cation and of the neutral species., respectively, and where $BE_{\text{core}}^{\text{cation,solid}}$ and $BE_{\text{core}}^{\text{neutral,solid}}$ are the binding energies (measured from the Fermi level) in the solid of the cation and of the neutral species, respectively.

A polarization energy P of $\sim$ 1.2 eV explains why the calculated energy difference of 3.8 eV between the cationic and neutral species calculated in the gas phase can be reduced to 1.5 eV in the solid state. Therefore, the charge transfer hypothesis must be regarded as likely. Nevertheless, we must check the consistency of two "charge state" model for the C 1s spectra.

Table 3. Calculated DFT $IE_{\text{core or valence}}^{\text{neutral,gas}}$ and $IE_{\text{core or valence}}^{\text{cation,gas}}$ values for the neutral and cationic DIPO-Ph_4 molecule. For the cationic form, core-ionized energies are calculated for the triplet final state. In the estimation of $BE_{\text{core or valence}}^{\text{cation,solid}} - BE_{\text{core or valence}}^{\text{neutral,solid}}$, the polarization energy P is taken as 1.2 eV (see Equation (2)).

Core/valence level Energy (eV)	**O 1s**	**C 1s Carb1 (phenyl)**	**C 1s Varb2 (ether)**	**C 1s Carb3 (central)**	**HOMO**
$IE_{\text{core or valence}}^{\text{neutral,gas}}$	537.67	289.25	290.70	289.14	5.14
$IE_{\text{core or valence}}^{\text{cation,gas}}$	541.47	292.00	294.27	293.02	8.49
$IE_{\text{core or valence}}^{\text{cation,gas}} - IE_{\text{core or valence}}^{\text{neutral,gas}}$	3.80	2.75	3.57	3.88	3.35
$BE_{\text{core or valence}}^{\text{cation,solid}} - BE_{\text{core or valence}}^{\text{neutral,solid}}$	1.40	0.35	1.2	1.5	1

In the DFT framework, we also calculate theoretically the C 1s $IE_{\text{core}}^{\text{neutral,gas}}$ and triplet-state $IE_{\text{core}}^{\text{cation,gas}}$ of selected atoms in the molecule. We distinguish three atoms, one labelled Carb1 pertains to the phenyl ring, and the two others pertain to the dipyranylidene core, Carb2 (central atoms) and Carb3 (ether bond), see Figure 1. The calculated energies are reported in Table 3. Via the HF approach, we have obtained that the singlet-state $IE_{\text{core}}^{\text{cation,gas}}$ is higher in energy than the triplet-state one by 0.2 and 0.4 eV for the

dipyranylidene carbons, Carb2 and Carb3, respectively (see SI, Section S9). Considering that the singlet state contributes to only 1/3 of the spectra weight and the rather small triplet-singlet energy shifts indicated by the HF calculation, spectra curve is mainly due to triplet-state.

For the neutral molecule, the triplet-state DFT IE of the central atoms is slightly shifted with respect to that of the phenyl carbons (by -0.1 eV), while that of the ether carbon is 1.5 eV higher, as experimentally observed. In contrast, for the cationic species, the IE of the central atoms is distinct from that of the phenyl by $+1$ eV. Physically, this means that the central carbons have lost charge, as it can be guessed from a representation of the HOMO (Figure 1). The ether carbon is found $+2.3$ eV higher than the phenyl, a sizeable increase when one considers the neutral molecule case.

Considering a polarization energy P of $\sim$ 1.2 eV that accounts for the solid effects, the energy difference $BE_{\text{core}}^{\text{cation,solid}} - BE_{\text{core}}^{\text{neutral,solid}}$ is reduced to $\sim$ 0.35 eV for the phenyl carbon. Consequently, peak C1 in Figure 3 can correspond to the phenyl carbons of both the neutral and cationic species. Component C2 at $\sim$ 1.2 eV from C1 can be attributed to the ether carbons of the neutral molecule and to the central carbons of the molecular cation, as $BE_{\text{core}}^{\text{cation,solid}} - BE_{\text{core}}^{\text{neutral,solid}}$ is worth $\sim$ 1.5 eV for the latter ones. Component C3 at 2.5 eV from C1 can be attributed to the ether carbons of the cation given that $BE_{\text{core}}^{\text{cation,solid}} - BE_{\text{core}}^{\text{neutral,solid}}$ is worth $\sim$ 1.2 eV. Consequently, the hypothesis of a mixture of neutral and cationic species in similar proportions consistently explains both the O 1s and C 1s spectra. Note that the O1/O2 proportions do not depend on the sample coverage as the island aureoles probed via XPS have the same area for the different sample from 1×10^{15} to 3×10^{15} molecule·cm^{-2}. Between the islands, no DIPO-Ph$_4$ material is thus deposited. Therefore, the DIPO-Ph$_4$ growth follows a Volmer-Weber mode.

2.3 Valence band energy levels

The valence band spectra of the chemically cleaned ITO substrate measured at a photon energy of 60 eV is presented in Figure 5(a), corresponding to a short IMFP (λ_{ITO} of $\sim$ 0.5 nm). From the valence band

edge, at a binding about 3 eV, a "tail" extends into the oxide gap. The origin of these gap states, that we observe up to about ~ 1.2 eV, see Figure 5(a_2), is yet unclear: mixed 5s/5p states of surface In^+ lone pairs, on the one hand, bulk oxygen vacancies and oxygen interstitials, on the other hand.[22,56,57] The valence band maximum energy (E_{VBM}) can be determined by fitting the valence band with two broad Gaussians, one representing the O 2p valence band edge and one the gap states,[20] see Figure 5(a_1). Then a value of ~ 3.14 eV for the O 2p E_{VBM} is determined. A comparison with the UPS and XPS measurements made by Gassenbauer *et al.* is relevant for the discussion on the band level scheme. The E_{VBM} value we find is bracketed between an E_{VBM} of ~ 3.54 eV for a magnetron-deposited reduced film (sputtering in argon, emission at Fermi level) and an E_{VBM} of ~ 2.94 eV for a film grown in more oxidative conditions (sputtering in 1% O_2/Ar no emission at Fermi level).[20] With an E_G value of ~ 2.9 eV, the $E_F - E_{\mathrm{VBM}}$ in the range 3.0 – 3.2 eV points to a Fermi level in the conduction band. This is consistent with the In $3d_{5/2}$ peak maximum at 444.63 eV that falls in between that of the film sputtered in pure Ar (444.93 eV, emission at Fermi level) and the one sputtered in the 1% O_2/Ar mixture (444.63 eV, no emission at Fermi level). Therefore, the In 5s states forming the conduction band should be occupied, considering the small E_G value that is now adopted. They do not appear clearly at $h\nu$ = 60 eV. However, they clearly show up using a much higher excitation energy of 850 eV (Figure 5(b)). Indeed, the conditions of their observation is optimized in the XPS regime, as the photoionization cross-section ration $\sigma_{\mathrm{In\ 5s}}/\sigma_{\mathrm{O\ 2p}}$ is 1.5 at a photon energy of 850 eV while it is only 3.1×10^{-2} at 60 eV.

We focus now on changes in the electronic structure due to DIPO-Ph_4 deposition. With respect to the substrate spectrum prior to deposition, the valence band spectra measured at $h\nu$ = 60 eV (Figure 5(a)) exhibit new features (red-, blue-, green- and violet-shaded components) related to the occupied molecular orbitals of DIPO-Ph_4 superimposed onto the ITO valence band contribution. Note that the valence band photoelectrons measured at this energy and the O 1s photoelectrons measured at $h\nu$ = 600 eV correspond to the same probing depth, as their KE (~ 60 eV and ~ 70 eV, respectively) are very close. Therefore, the two chemical states associated to the O1 and O2 components in the O 1s spectrum contribute in nearly equal weights to the molecular valence band spectrum.

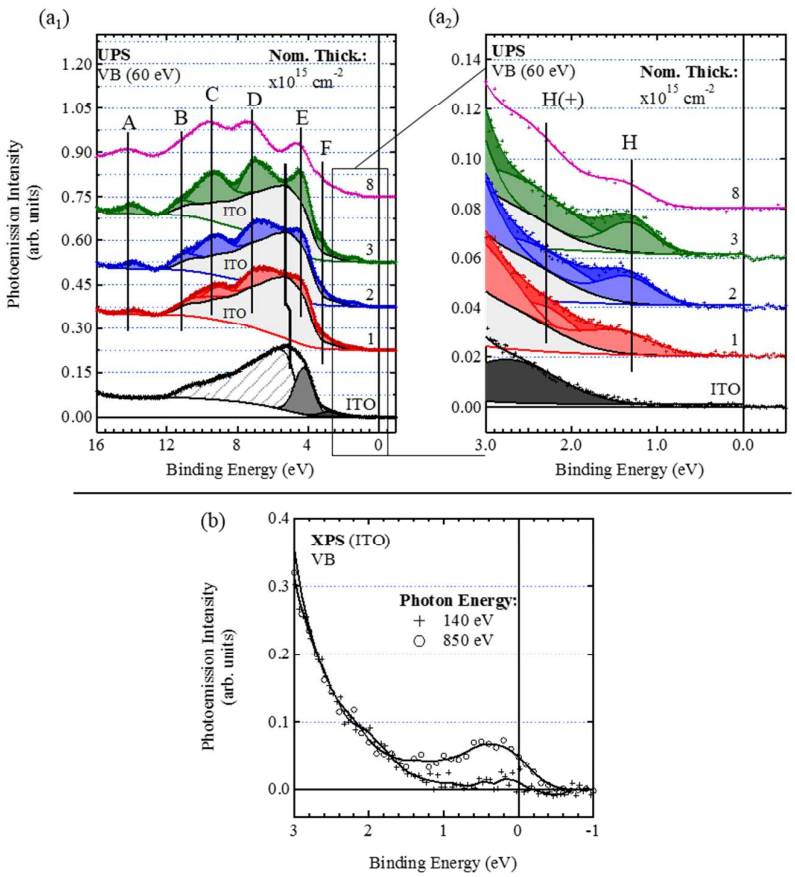

Figure 5. UV photoemission: (a_1) ITO and DIPO-Ph_4 maximum valence band with HOMO levels of DIPO-Ph_4 and (a_2) zoom on the ITO gap states. Coverages in molecule·cm^{-2} are obtained from QB measurements. The ITO contribution for all samples, except the thickest deposit of 8×10^{15} molecule·cm^{-2}, is represented by the grey-shaded area (labelled ITO). H is the HOMO of the neutral molecule, and H(+) indicates the binding energy of the cation singly occupied molecular orbital (SOMO). (b) Soft X-ray valence band photoemission of the bare ITO surface at a photon energy of 850 eV: states appear at Fermi Level due to the increase in the $\sigma_{\text{In 5s}}/\sigma_{\text{O 2p}}$ ratio.

For deposits $\leq 3\times10^{15}$ molecule·cm^{-2}, a grey-shaded synthetic spectrum represents the ITO contribution This is the major one in the valence spectra. At $h\nu$ = 60 eV, the IMFP $\lambda_{\text{DIPO-Ph}_4}$ of the photoelectron in the molecular solid is only ~ 0.55 nm. Considering the morphology of the deposit, the photoemission signal comes from the top of the molecular mounds and from the inter-mound areas, that represents still 40% of the surface for a deposit of 3×10^{15} molecule·cm^{-2}. The probed ITO still shows its metallic character (there is a weak Fermi level emission for the 3×10^{15} molecule·cm^{-2} deposit). The valence band spectrum of the thickest deposit (8×10^{15} molecule·cm^{-2}) is more characteristic of the organic material as the ITO contribution in the O 1s spectrum (Figure 4(c)) is minimal, and the neutral state corresponds to

70% of the molecular spectral weight. We observe the growth of six strong components, labeled A to F, that show up at BE 14.06, 10.97, 9.36, 6.99, 4.30, 3.29 eV, respectively, plus two molecular states that appear in the ITO gap centered at 2.5 eV and 1.4 eV, that we denote H(+) and H, respectively.

As the measured spectrum results from the combination of two different chemical states (neutral versus cationic) of the molecule, the respective molecular levels are mixed up in the experimental spectrum. Let us now start with the two molecular levels with lower BE, H(+) and H that appear in the gap of ITO. Using DFT, we have calculated the vertical valence ionization energy of the highest occupied molecular orbital (HOMO, neutral) and singly occupied molecular orbital (SOMO, cationic), $IE_{\mathrm{HOMO}}^{\mathrm{neutral,gas}}$ and $IE_{\mathrm{SOMO}}^{\mathrm{cation,gas}}$, respectively. We find $IE_{\mathrm{HOMO}}^{\mathrm{neutral,gas}}$ = 5.14 eV and $IE_{\mathrm{SOMO}}^{\mathrm{cation,gas}}$ = 8.49 eV. The DFT energy difference $IE_{\mathrm{SOMO}}^{\mathrm{cation,gas}} - IE_{\mathrm{HOMO}}^{\mathrm{neutral,gas}}$ (Table 3) is close to that calculated for the (triplet state) C 1s core-levels of atoms in the dipyranylidene core. The estimated BE energy difference in the solid state $BE_{\mathrm{SOMO}}^{\mathrm{cation,solid}} - BE_{\mathrm{HOMO}}^{\mathrm{neutral,solid}}$ is reduced ~ 1 eV with P equal to ~ 1.2 eV (Equation (2)). Therefore, the components and H(+) and H, whose measured BE difference is also ~ 1 eV, are attributed to the SOMO level of the cationic species and to the HOMO of the neutral molecule, respectively.

We have tried to calculate the DFT ionization energy of molecular orbitals (neutral and cationic state) that are essentially localized on phenyls. The calculation of the doubly ionized states does not converge, because the phenyl localized orbitals pertain to a manifold of levels with very close energies. Nevertheless, the difference in the ionization energies between the neutral state and the cationic state may be expected to be lower than in the case of the highest energy levels (HOMO and SOMO), since the charge appearing on the phenyl is spatially remote from the electron vacancy localized on the core of the molecule. The latter point is clearly demonstrated by the valence band spectra of films of 2,2',6,6'-tetraphenyl-4,4'-dithiadipyranylidene (DIPS-Ph_4) we present in Figure S9 of the SI, Section S11. In DIPS-Ph_4 the two oxygen atoms of DIPO-Ph_4 (see Figure 1) are substituted by two sulphur atoms, and the molecular orbitals are very similar. We have successfully prepared a very thick layer (13×10^{15} molecule·cm^{-2}), for which only the neutral state is seen, as proved by a single spin-orbit split doublet in

the S 2p spectra. We label the molecular components A – F and H, as for the DIPO-Ph_4 molecule. We observe a clear narrow HOMO level well isolated from the A – F series.

2.4 Electron energy level scheme of the ITO/DIPO-Ph_4 interface

To complete the electronic level scheme of the ITO/DIPO-Ph_4 interface, work function (Φ) measurements are determined via the measurement of the cutoff of secondary electron energy distribution curves (SEEDC). We find Φ equal to 4.20 eV for the bare substrate (see Figure S10). The SEEDC of the deposits 10^{15}, 2×10^{15} and 3×10^{15} molecule·cm^{-2} give a Φ value of 3.90 eV, independent of coverage (in the thick limit). The slight decrease in work-function associated to molecular adsorption can be attributed to the formation of cationic species at the ITO/DIPO-Ph_4 interface.[16]

We present in Figure 6, the electron energy level scheme of the ITO/DIPO-Ph_4 interface. The important parameters are the E_F − HOMO (neutral) energy offset of 0.7eV (leading edge)/1.4 eV (centroid), the molecular solid work function Φ (3.90 eV), and the valence ionization energy of DIPO-Ph_4 is obtained by adding Φ to the HOMO binding energy measured from the Fermi level to give 4.6 eV (HOMO leading edge)/ 5.3 eV (centroid). The SOMO level of the cationic species H(+) has a higher binding energy (referenced to the Fermi level) and thus a higher ionization energy (referenced to the vacuum level) that of the neutral HOMO level, as demonstrated by the DFT calculation of the isolated molecule (see section 2.3) As emphasized in Ref. 58 UPS generates photoemitted electrons that carry away with them the relaxation energies (electronic polarization and structural relaxation) of the valence ionized molecule. This is entirely true for molecules in the neutral ground state, and therefore the measured HOMO binding energies are relevant to discuss transport properties, in particular the transport gap of molecular solids, when inverse photoemission spectroscopy data about the lowest unoccupied molecular orbital (LUMO) energy are also available. However, as E_F approaches the HOMO this molecular level is partly emptied due to a charge transfer to the substrate, but the spectroscopic level H(+) (a doubly ionized final state) will appear below the HOMO due to the strong hole-hole interaction. This is a common observation in

UPS spectroscopy, when SOMOs are concerned (a good example is the valence band spectroscopy of copper phthalocyanine[59]).

Let us first consider the E_F − HOMO (neutral) energy offset. As the HOMO (neutral) is below the Fermi level by at least 0.7 eV (edge), there is no barrier to collect holes from the DIPO-Ph_4 layer into the ITO substrate, as expected. It is also worth noticing that E_F − HOMO (neutral) is also the hole *injection* barrier (Δ_h) from ITO to the molecular solid. The low value of 0.7 eV (edge) make it interesting for organic light emitting diodes, and very competitive with other organic hole-transport materials such as TPD and α-NPD deposited on ITO.[60]

Now, could the DIPO-Ph_4 layer be an efficient interfacial hole collecting layer *per se* in the context of the state-of-the-art bulk heterojunctions (BHJ) of organic photovoltaic? The BHJ are blends of hole-transport P3HT and electron transport PCBM. Some predictions can be made from the present data and from already published UPS[61,62] and inverse photoemission spectroscopy (IPES) works.[62] The expected energy level schemes of the interfaces are given in Figure 6.

Vacuum-level alignment should be obeyed at the DIPO-Ph_4/P3HT interface. Indeed, the work function of P3HT is 3.9 eV[61] (identical to that of DIPO-Ph_4) and its ionization energy (HOMO edge) is 4.65 eV.[62] As the ionization energy (HOMO edge) of DIPO-Ph_4 is 4.6 eV then the HOMOs of the two materials are practically coincident. Therefore, the injection of holes from P3HT to ITO *via the DIPO-Ph_4 interfacial layer* remains barrierless.

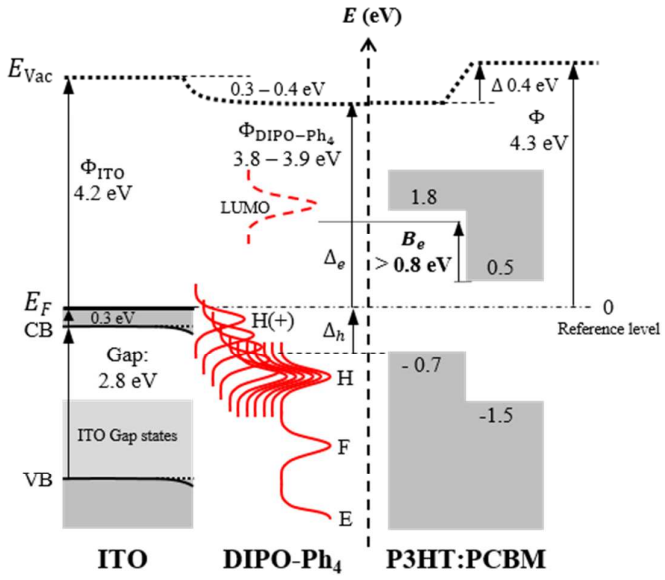

Figure 6. Expected energy level scheme of the ITO/DIPO-Ph_4/P3HT:PCBM system. The work functions of DIPO-Ph_4 and of P3HT[61] are both equal to 3.9 eV (and coincidentally the vacuum levels are aligned). The HOMO energy versus E_{vac} (vacuum level) in P3HT is from Ref. 62. The Fermi level in metallic ITO, P3HT and PCBM[61] are assumed to be aligned. Δ is the energy offset. The LUMO/HOMO energies versus vacuum are from Ref. 62. As the LUMO − HOMO gap in DIPO-Ph_4 is greater than 2 eV (Figure S1) the minimum electron blocking barrier $B_e^{\min}$ is 0.8 eV. E_F and E_{vac} are the Fermi and vacuum level, respectively (E_F is the zero of energies).

The interfacial DIPO-Ph_4 may also come into contact with PCBM. Figure 6 shows the expected energy level scheme at DIPO-Ph_4/PCBM interface. The work function of DIPO-Ph_4 donor (3.9 eV) is smaller than that of the PCBM acceptor, 4.3 eV.[61] Therefore electron charge should be transferred from DIPO-Ph_4 to PCBM, after level alignment, an energy offset Δ of $\sim +0.4$ eV appears.[61,63] This offset (generally ignored in most depictions of the energy schemes of these photovoltaic materials) will bring up the PCBM LUMO in energy and make it closer to that of DIPO-Ph_4. Considering that transport gap in DIPO-Ph_4 is greater than 2 eV (the value of the optical gap, see Figure S1), and considering that the PCBM LUMO is 3.8 eV below the vacuum level,[62] then the LUMO (DIPO-Ph_4)/LUMO (PCBM) energy difference is greater than 0.8 eV. Therefore DIPO-Ph_4 should remain an efficient blocking barrier (B_e) to electrons coming from PCBM despite the positive value of Δ.

To sum up, the DIPO-Ph_4 interfacial layer presents a favorable energy level scheme to collect holes from P3HT and to block electrons from PCBM. However, if this condition is necessary, it is not sufficient for

the material to behave as an efficient hole collector, and to improve the performances of the BHJ cells. The conductivity of the DIPO-Ph_4 material and the number of good "contact" points with the ITO substrate (per surface unit) must be also high. In the case of the parent molecule DIPS-Ph_4, CS-AFM points to a sizeable increase in hole-carrying pathways with respect to PEDOT:PSS.[12]

Given the UHV deposition conditions, DIPO-Ph_4 should be undoped and moderately conductive. It is only when it meets the substrate that it can transfer electronic charge and become a cation. This is a particular case of doping different from the classical molecular doping,[64–66] where acceptor or donor molecules are inserted into the organic semiconductor host. A significant difference with molecular doping is the absence of negatively charged recombination centers in the film itself. Thin layers in contact with the substrate may have a high hole conductivity.

Conclusive remarks

We combine AFM and synchrotron radiation XPS/UPS to elucidate the formation the ITO/DIPO-Ph_4 interface, DIPO-Ph_4 has appeared as a very promising interfacial layer for hole collection in organic photovoltaics. The ITO/DIPO-Ph_4 morphology of the deposits otherwise characterized by XPS/UPS, is examined by AFM. For coverages in the 1×10^{15} – 8×10^{15} molecule·cm^{-2} range, we do not observe a layer-by-layer growth mode. Molecular mounds are formed, starting from ITO macroscopic surface defects. In the 1×10^{15} – 3×10^{15} molecule·cm^{-2} range the height of the mounds is typically 30 nm, leaving inter-mound area bare or covered by an ultrathin layer that remains unobservable by AFM. Only at 8×10^{15} molecule·cm^{-2} does the mounds tend to coalesce, and their height reaches an average value of 50 nm.

Synchrotron radiation XPS and UPS give unique information on the electronic properties of both the substrate and the film. The fact that the film thickness is not uniform, as shown by AFM, is crucial to interpret the photoemission spectra. Indeed, for coverages $\leq 3\times10^{15}$ molecule·cm^{-2}, a sizeable ITO contribution is always observed in the O 1s and valence band spectra, even in highly surface sensitive

conditions. The ITO-related signal originates from the inter-mound areas (and the aureoles of the mound) where the deposit thickness is very thin. All substrate related components (*e.g.* In 3d) increase their binding energies when the molecule is deposited, indicating that the Fermi level moves up in energy due to the interaction with the molecule. This may be interpreted as a filling of the conduction band by electrons coming from the deposited molecules.

For all the deposits studied, we detect the presence of two components in the O 1s spectra, indicating that the molecule is in two different states. One state corresponds to an ether oxygen of an otherwise unaltered molecule. The second one at higher binding energy originates from an altered molecule interacting with the substrate. These two molecular states are in comparable amounts until the DIPO-Ph_4 mounds almost coalesce. Then the relative weight of the altered state at high binding energy diminishes. The fact that the altered species gives a sizeable spectra contribution, even in surface sensitive conditions, is due to the growth mode: its signal comes from the inter-mound areas and from the flanks of the mounds, where the layer thickness become comparable to the probed length. Given than the DIPO-Ph_4 is an excellent donor, the possibility of a molecular cation is examined. O 1s core-ionized state DFT calculations of isolated molecules in the neutral and cationic state give a reasonable explanation for the observed O 1s binding energy difference when the core-hole relaxation energy in dielectric media is accounted for. The C 1s spectra can also be interpreted in a similar way.

The UPS valence band of the bare substrate is characteristic of metallic ITO, with a density of state observable at Fermi level. When the molecule is deposited, new states appear. The corresponding molecular levels are also interpreted within the framework of the two molecular states, neutral and cationic. The HOMO of the neutral molecule shows up, centered at 1.4 eV below the Fermi level with its edge only 0.7 eV below the Fermi level. The HOMO of the cationic species is found shifted to higher binding energy by ~ 1.1 eV (centroid at ~ 2.5 eV below the Fermi level). The work function of the ITO surface is affected by a slight decrease when the molecule is deposited (~ 0.3 eV), due to the charge transfer from the molecule to the substrate. The work function of the deposit (3.9 eV) is therefore the integer charge transfer energy.

Finally, we draw the electron level the ITO/DIPO-Ph_4 interface, and discuss the implications in devices, as a hole conducting layer in organic light emitting diodes and as an anode interfacial layer in organic solar cells.

Supporting information

The UV absorption and the elementary analysis of DIPO-Ph_4, the calculated inelastic mean free paths of both the organic material and the substrate, the detailed In 3d, In 4d and Sn 4d ITO core levels, the beam damage control, the original O 1s peak at 825 eV, the Sn 3d spectra and the work function measurements of the ITO/DIPO-Ph_4 interface, the details on the theoretical calculations, and the valence band spectra of DIPS-Ph_4 are supplied as Supporting information.

Acknowledgement

QA thanks LABEX MiChem for funding his PhD grant. The authors express their thanks to TEMPO and ALOISA beamline teams (SOLEIL and ELETTRA synchrotrons) for their very efficient technical support.

References

(1) Klein, A. Transparent Conducting Oxides: Electronic Structure-Property Relationship from Photoelectron Spectroscopy with in Situ Sample Preparation. *J. Am. Ceram. Soc.* **2013**, *96* (2), 331–345.

(2) Brabec, C.; Dyakonov, V.; Scherf, U. *Organic Photovoltaics: Materials, Device Physics, and Manufacturing Technologies*; Brabec, C., Dyakonov, V., Scherf, U., Eds.; Wiley-VCH Verlag GmbH & Co. KGaA: Weinheim, Germany, 2009, 1st edition.

(3) Hains, A. W.; Liang, Z.; Woodhouse, M. A.; Gregg, B. A. Molecular Semiconductors in Organic Photovoltaic Cells. *Chem. Rev.* **2010**, *110* (11), 6689–6735.

(4) Meiss, J.; Uhrich, C. L.; Fehse, K.; Pfuetzner, S.; Riede, M. K.; Leo, K. Transparent Electrode Materials for Solar Cells. In *Photonics Europe, Photonics for solar Energy Systems II*; Schelkens, P., Gombert, A., Berghmans, F., Tervonen, A., De La Rue, R. M., Andrews, D. L., Kalli, K., Popp, J., Johnson, N. P., Urey, H., et al., Eds.; 2008; Vol. 7002, pp 700210–700218.

(5) Hyesung, P.; Rowehl, J. A.; Ki Kang, K.; Bulovic, V.; Jing, K. Doped Graphene Electrodes for Organic Solar Cells. *Nanotechnology* **2010**, *21* (50), 505204–505209.

(6) Zhu, Y.; Sun, Z.; Yan, Z.; Jin, Z.; Tour, J. M. Rational Design of Hybrid Graphene Films for High-Performance Transparent Electrodes. *ACS Nano* **2011**, *5* (8), 6472–6479.

(7) Johnson, D. Graphene Still Trying to Replace ITO in Organic Solar Cells spectrum.ieee.org (accessed Jun 26, 2017).

(8) Mirletz, H. M.; Peterson, K. A.; Martin, I. T.; French, R. H. Degradation of Transparent Conductive Oxides: Interfacial Engineering and Mechanistic Insights. *Sol. Energy Mater. Sol. Cells* **2015**, *143*, 529–538.

(9) Yeo, J. S.; Yun, J. M.; Kang, M.; Khim, D.; Lee, S. H.; Kim, S. S.; Na, S. I.; Kim, D. Y. An Approach for an Advanced Anode Interfacial Layer with Electron-Blocking Ability to Achieve High-Efficiency Organic Photovoltaics. *ACS Appl. Mater. Interfaces* **2014**, *6* (22), 19613–19620.

(10) Irwin, M. D.; Buchholz, D. B.; Hains, A. W.; Chang, R. P. H.; Marks, T. J. P-Type Semiconducting Nickel Oxide as an Efficiency-Enhancing Anode Interfacial Layer in Polymer Bulk-Heterojunction Solar Cells. *Proc. Natl. Acad. Sci.* **2008**, *105* (8), 2783–2787.

(11) Zeng, H.; Zhu, X.; Liang, Y.; Guo, X. Interfacial Layer Engineering for Performance Enhancement in Polymer Solar Cells. *Polymers (Basel).* **2015**, *7* (2), 333–372.

(12) Berny, S.; Tortech, L.; Véber, M.; Fichou, D. Dithiapyrannylidenes as Efficient Hole Collection Interfacial Layers in Organic Solar Cells. *ACS Appl. Mater. Interfaces* **2010**, *2* (11), 3059–3068.

(13) Kahn, A.; Koch, N.; Gao, W. Electronic Structure and Electrical Properties of Interfaces between Metals and Pi-Conjugated Molecular Films. *J. Polym. Sci. Part B Polym. Phys.* **2003**, *41* (21), 2529–2548.

(14) Crispin, X.; Geskin, V.; Crispin, A.; Cornil, J.; Lazzaroni, R.; Salaneck, W. R.; Brédas, J. L. Characterization of the Interface Dipole at Organic/metal Interfaces. *J. Am. Chem. Soc.* **2002**, *124* (27), 8131–8141.

(15) Braun, S.; Osikowicz, W.; Wang, Y.; Salaneck, W. R. Energy Level Alignment Regimes at Hybrid Organic-Organic and Inorganic-Organic Interfaces. *Org. Electron. physics, Mater. Appl.* **2007**, *8* (1), 14–20.

(16) Braun, S.; Salaneck, W. R.; Fahlman, M. Energy-Level Alignment at Organic/metal and Organic/organic Interfaces. *Adv. Mater.* **2009**, *21* (14–15), 1450–1472.

(17) Khaliq, A.; Gallet, J. J.; Bournel, F.; Pierucci, D.; Tissot, H.; Silly, M.; Sirotti, F.; Rochet, F. Charge Transfer and Energy Level Alignment at the Interface between Cyclopentene-Modified Si(001) and Tetracyanoquinodimethane. *J. Phys. Chem. C* **2014**, *118* (39), 22499–22508.

(18) Vázquez, H.; Flores, F.; Kahn, A. Induced Density of States Model for Weakly-Interacting Organic Semiconductor Interfaces. *Org. Electron. physics, Mater. Appl.* **2007**, *8* (2–3), 241–248.

(19) Oehzelt, M.; Koch, N.; Heimel, G. Organic Semiconductor Density of States Controls the Energy Level Alignment at Electrode Interfaces. *Nat. Commun.* **2014**, *5*, 4174–4181.

(20) Gassenbauer, Y.; Schafranek, R.; Klein, A.; Zafeiratos, S.; Hävecker, M.; Knop-Gericke, A.; Schlögl, R. Surface States, Surface Potentials, and Segregation at Surfaces of Tin-Doped In2O3. *Phys. Rev. B - Condens. Matter Mater. Phys.* **2006**, *73* (24), 245312–245322.

(21) Walsh, A.; Da Silva, J. L. F.; Wei, S. H.; Körber, C.; Klein, A.; Piper, L. F. J.; Demasi, A.; Smith, K. E.; Panaccione, G.; Torelli, P.; et al. Nature of the Band Gap of In2O3 Revealed by First-Principles Calculations and X-Ray Spectroscopy. *Phys. Rev. Lett.* **2008**, *100* (16), 167402–167405.

(22) Braun, D.; Scherer, V.; Janowitz, C.; Galazka, Z.; Fornari, R.; Manzke, R. In-Gap States of In2O3 Single Crystals Investigated by Scanning Tunneling Spectroscopy. *Phys. Status Solidi Appl. Mater. Sci.* **2014**, *211* (1), 59–65.

(23) Burstein, E. Anomalous Optical Absorption Limit in InSb4. *Phys. Rev.* **1954**, *93* (3), 632–633.

(24) Moss, T. S. The Interpretation of the Properties of Indium Antimonide. *Proc. Phys. Soc. Sect. B* **1954**, *67* (10), 775–782.

(25) Klein, A.; Körber, C.; Wachau, A.; Säuberlich, F.; Gassenbauer, Y.; Harvey, S. P.; Proffit, D. E.; Mason, T. O. Transparent Conducting Oxides for Photovoltaics: Manipulation of Fermi Level,work Function and Energy Band Alignment. *Materials (Basel).* **2010**, *3* (11), 4892–4914.

(26) Körber, C.; Krishnakumar, V.; Klein, A.; Panaccione, G.; Torelli, P.; Walsh, A.; Da Silva, J. L. F.; Wei, S.-H.; Egdell, R. G.; Payne, D. J. Electronic Structure of In2O3 and Sn-Doped In2O3 by Hard X-Ray Photoemission Spectroscopy. *Phys. Rev. B* **2010**, *81* (16), 165207–165215.

(27) Fichou, D.; Tortech, L.; Alaaeddine, M. Nouveau Procédé de Fabrication de Dispositifs Électroniques Organiques, 2014.

(28) Alizon, J.; Blanc, J.; Gallice, J.; Robert, H.; Fabre, C.; Strzelecka, H.; Rivory, J.; Weyl, C. Investigations of High Conductivity of Dipyranylidene and Dithiadipyranylidene — TCNQ Complexes. In *Organic Conductors and Semiconductors*; Pál, L., Grüner, G., Jánossy, A., Sólyom, J., Eds.; Lecture Notes in Physics; Springer-Verlag: Berlin/Heidelberg, Heidelberg, 1977; pp 563–569.

(29) D'Andrade, B. W.; Datta, S.; Forrest, S. R.; Djurovich, P.; Polikarpov, E.; Thompson, M. E.

Relationship between the Ionization and Oxidation Potentials of Molecular Organic Semiconductors. *Org. Electron. physics, Mater. Appl.* **2005**, *6* (1), 11–20.

(30) Barth, V. Dipyrrométhènes Métallés (Co,Ni,Cu) et Dipyrannilidènes : De Nouveaux Matériaux Organiques Pour La Conversion Photovoltaïque de L'énergie Solaire, Paris 6, 2014.

(31) Chasseau, D.; Gaultier, J.; Hauw, C.; Fugnitto, R.; Gianis, V.; Strzelecka, H. Tétraphényldipyranylidène (Dip φ4). *Acta Crystallogr. Sect. B* **1982**, *38* (5), 1629–1631.

(32) Mason, M. G.; Hung, L. S.; Tang, C. W.; Lee, S. T.; Wong, K. W.; Wang, M. Characterization Of Treated Indium–Tin–Oxide Surfaces Used In Electroluminescent Devices. *J. Appl. Phys.* **1999**, *86* (3), 1688–1692.

(33) Lo, M. F.; Ng, T. W.; Mo, H. W.; Lee, C. S. Direct Threat of a UV-Ozone Treated Indium-Tin-Oxide Substrate to the Stabilities of Common Organic Semiconductors. *Adv. Funct. Mater.* **2013**, *23* (13), 1718–1723.

(34) Klein, A. Energy Band Alignment at Interfaces of Semiconducting Oxides: A Review of Experimental Determination Using Photoelectron Spectroscopy and Comparison with Theoretical Predictions by the Electron Affinity Rule, Charge Neutrality Levels, and the Common Anion. *Thin Solid Films* **2012**, *520* (10), 3721–3728.

(35) Berny, S.; Tortech, L.; Fichou, D. Derives de Type Dipyrannylidene Comme Couche Interfaciale Anodique Dans Des Dispositifs Electroniques. 2011.

(36) Campbell, J. L.; Papp, T. Widths of the Atomic K–N7 Levels. *At. Data Nucl. Data Tables* **2001**, *77* (1), 1–56.

(37) Hwang, J.; Wan, A.; Kahn, A. Energetics of Metal-Organic Interfaces: New Experiments and Assessment of the Field. *Mater. Sci. Eng. R Reports* **2009**, *64* (1–2), 1–31.

(38) Gassmann, J.; Yampolskii, S. V.; Genenko, Y. A.; Reusch, T. C. G.; Klein, A. Functional

Interfaces for Transparent Organic Electronic Devices: Consistent Description of Charge Injection by Combining In Situ XPS and Current Voltage Measurements with Self-Consistent Modeling. *J. Phys. Chem. C* **2016**, *120* (19), 10466–10475.

(39) Jablonski, A. Determination of the Electron Inelastic Mean Free Path in Solids from the Elastic Electron Backscattering Intensity. *Surf. Interface Anal.* **2005**, *37* (11), 1035–1044.

(40) Powell, C. J.; Jablonski, A. Surface Sensitivity of X-Ray Photoelectron Spectroscopy. *Nucl. Instruments Methods Phys. Res. Sect. A Accel. Spectrometers, Detect. Assoc. Equip.* **2009**, *601* (1–2), 54–65.

(41) Venables, J. A.; Spiller, G. D. T.; Hanbucken, M. Nucleation and Growth of Thin Films. *Reports Prog. Phys.* **1984**, *47* (4), 399–459.

(42) Ibach, H.; Lüth, H. *Solid-State Physics: An Introduction to Principles of Materials Science*; Springer; 2nd edition, 2010.

(43) Qi, D.; Chen, W.; Gao, X.; Wang, L.; Chen, S.; Kian, P. L.; Wee, A. T. S. Surface Transfer Doping of Diamond (100) by Tetrafluoro- Tetracyanoquinodimethane. *J. Am. Chem. Soc.* **2007**, *129* (26), 8084–8085.

(44) Barr, T. L. Nature of the Use of Adventitious Carbon as a Binding Energy Standard. *J. Vac. Sci. Technol. A Vacuum, Surfaces, Film.* **1995**, *13* (3), 1239–1246.

(45) Bermudez, V. M.; Berry, A. D.; Kim, H.; Piqué, A. Functionalization of Indium Tin Oxide. *Langmuir* **2006**, *22* (26), 11113–11125.

(46) Harvey, S. P.; Mason, T. O.; Gassenbauer, Y.; Schafranek, R.; Klein, A. Surface versus Bulk Electronic/defect Structures of Transparent Conducting Oxides: I. Indium Oxide and ITO. *J. Phys. D. Appl. Phys.* **2006**, *39* (18), 3959–3968.

(47) López, G. P.; Castner, D. G.; Ratner, B. D. XPS O 1s Binding Energies for Polymers Containing

Hydroxyl, Ether, Ketone and Ester Groups. *Surf. Interface Anal.* **1991**, *17* (5), 267–272.

(48) Gassenbauer, Y.; Klein, A. Electronic and Chemical Properties of Tin-Doped Indium Oxide (ITO) Surfaces and ITO/ZnPc Interfaces Studied in-Situ by Photoelectron Spectroscopy. *J. Phys. Chem. B* **2006**, *110* (10), 4793–4801.

(49) Hirose, Y.; Kahn, A.; Aristov, V.; Soukiassian, P. Chemistry, Diffusion, and Electronic Properties of a Metal/organic Semiconductor Contact: In/perylenetetracarboxylic Dianhydride. *Appl. Phys. Lett.* **1996**, *68* (2), 217–219.

(50) Hirose, Y.; Kahn, A.; Aristov, V.; Soukiassian, P.; Bulovic, V.; Forrest, S. R. Chemistry and Electronic Properties of Metal-Organic Semiconductor Interfaces: Al, Ti, In, Sn, Ag, and Au on PTCDA. *Phys. Rev. B* **1996**, *54* (19), 13748–13758.

(51) Carniato, S.; Gallet, J. J.; Rochet, F.; Dufour, G.; Bournel, F.; Rangan, S.; Verdini, A.; Floreano, L. Characterization of Hydroxyl Groups on Water-Reacted Si (001)-2x1 Using Synchrotron Radiation O 1s Core-Level Spectroscopies and Core-Excited State Density-Functional Calculations. *Phys. Rev. B - Condens. Matter Mater. Phys.* **2007**, *76* (8), 085321–085333.

(52) Coustel, R.; Carniato, S.; Rochet, F.; Witkowski, N. Pyridine on Si(001)-(2x1): Density Functional Theory Simulations Compared with Spectroscopic Measurements. *Phys. Rev. B - Condens. Matter Mater. Phys.* **2012**, *85* (3), 035323–035331.

(53) Carniato, S.; Rochet, F.; Gallet, J. J.; Bournel, F.; Dufour, G.; Mathieu, C.; Rangan, S. DFT Calculations of XPS/NEXAFS and IR Spectra to Elucidate the Reaction Products of Acetonitrile with Si(001)-2x1. *Surf. Sci.* **2007**, *601* (23), 5515–5525.

(54) Mathieu, C.; Bai, X.; Gallet, J. J.; Bournel, F.; Carniato, S.; Rochet, F.; Magnano, E.; Bondino, F.; Funke, R.; Köhler, U.; et al. Molecular Staples on Si(001)-2x1: Dual-Head Primary Amines. *J. Phys. Chem. C* **2009**, *113* (26), 11336–11345.

(55) Rangan, S.; Bournel, F.; Gallet, J. J.; Kubsky, S.; Le Guen, K.; Dufour, G.; Rochet, F.; Sirotti, F.; Carniato, S.; Ilakovac, V. Experimental and Theoretical NEXAFS/XPS Study of the Room-Temperature Adsorption of Acetonitrile on Si (001) -2x1. *Phys. Rev. B - Condens. Matter Mater. Phys.* **2005**, *71* (16), 165319–165329.

(56) Egdell, R. G. Dopant and Defect Induced Electronic States at In2O3 Surfaces. In *Springer Series in Surface Sciences*; Jupille, J., Thornton, G., Eds.; Springer Series in Surface Sciences; Springer International Publishing, 2015; Vol. 58, pp 351–400.

(57) Ágoston, P.; Erhart, P.; Klein, A.; Albe, K. Geometry, Electronic Structure and Thermodynamic Stability of Intrinsic Point Defects in Indium Oxide. *J. Phys. Condens. Matter* **2009**, *21* (45), 455801–455811.

(58) Cahen, D.; Kahn, A. Electron Energetics at Surfaces and Interfaces: Concepts and Experiments. *Adv. Mater.* **2003**, *15* (4), 271–277.

(59) Evangelista, F.; Carravetta, V.; Stefani, G.; Jansik, B.; Alagia, M.; Stranges, S.; Ruocco, A. Electronic Structure of Copper Phthalocyanine: An Experimental and Theoretical Study of Occupied and Unoccupied Levels. *J. Chem. Phys.* **2007**, *126* (12), 124709–124718.

(60) Milliron, D. J.; Hill, I. G.; Shen, C.; Kahn, A.; Schwartz, J. Surface Oxidation Activates Indium Tin Oxide for Hole Injection. *J. Appl. Phys.* **2000**, *87* (1), 572–576.

(61) Xu, Z.; Chen, L.; Chen, M.; Li, G.; Yang, Y. Energy Level Alignment of poly(3-Hexylthiophene): [6,6]-Phenyl C-61 Butyric Acid Methyl Ester Bulk Heterojunction. *Appl. Phys. Lett.* **2008**, *95* (1), 13301–13303.

(62) Guan, Z.-L.; Kim, J. B.; Wang, H.; Jaye, C.; Fischer, D. A.; Loo, Y.-L.; Kahn, A. Direct Determination of the Electronic Structure of the poly(3-Hexylthiophene):phenyl-[6,6]-C61 Butyric Acid Methyl Ester Blend. *Org. Electron.* **2010**, *11* (11), 1779–1785.

(63) Chen, Q.; Mao, L.; Li, Y.; Kong, T.; Wu, N.; Ma, C.; Bai, S.; Jin, Y.; Wu, D.; Lu, W.; et al. Quantitative Operando Visualization of the Energy Band Depth Profile in Solar Cells. *Nat. Commun.* **2015**, *6*, 7745–7753.

(64) Lee, J. H.; Kim, J. J. Interfacial Doping for Efficient Charge Injection in Organic Semiconductors. *Phys. Status Solidi Appl. Mater. Sci.* **2012**, *209* (8), 1399–1413.

(65) Yoo, S. J.; Kim, J. J. Charge Transport in Electrically Doped Amorphous Organic Semiconductors. *Macromol. Rapid Commun.* **2015**, *36* (11), 984–1000.

(66) Lüssem, B.; Riede, M.; Leo, K. Doping of Organic Semiconductors. *Phys. Status Solidi Appl. Mater. Sci.* **2013**, *210* (1), 9–43.